Università di Pisa

Analytical Model of One-Dimensional Carbon-Based Schottky-Barrier Transistors

Paolo Michetti
Dipartimento di Ingegneria dell'Informazione: Elettronica, Informatica, Telecomunicazioni, Università di Pisa
Giuseppe Iannaccone
Dipartimento di Ingegneria dell'Informazione: Elettronica, Informatica, Telecomunicazioni, Università di Pisa

P.Michetti, G.Iannaccone, *Analytical Model of One-Dimensional Carbon-Based Schottky-Barrier Transistors*, IEEE Transactions on Electron Devices, **57**, 7, pp. 1616 – 1625, (2010)

Analytical Model of One-Dimensional Carbon-Based Schottky-Barrier Transistors

Paolo Michetti and Giuseppe Iannaccone, *Senior Member, IEEE*

***Abstract*—Nanotransistors typically operate in far-from-equilibrium (FFE) conditions, which cannot be described neither by drift diffusion nor by purely ballistic models. In carbon-based nanotransistors, source and drain contacts are often characterized by the formation of Schottky barriers (SBs), with strong influence on transport. In this paper, we present a model for 1-D field-effect transistors, taking into account on equal footing both SB contacts and FFE transport regime. Intermediate transport is introduced within the Büttiker's probe approach to dissipative transport, in which a nonballistic transistor is seen as a suitable series of individually ballistic channels. Our model permits the study of the interplay of SBs and ambipolar FFE transport and, in particular, of the transition between SB- and dissipation-limited transports.**

***Index Terms*—Ballistic transport, Büttiker probes, carbon nanotubes (CNTs), carbon transistors, compact model, far-from-equilibrium (FFE) transport, graphene, Schottky barrier (SB).**

I. Introduction

SINCE THE isolation of graphene in sheets [1], [2], with their exceptionally promising high mobility [3], graphene-related materials have attracted much interest for their possible application in nanoelectronic devices. In particular, semiconducting carbon nanotubes (CNTs) [4] and single-layer or bilayer graphene nanoribbons (GNRs) [5] have been successfully employed in quasi-1-D nanotransistors.

An important issue related to carbon-based channels is the nature of metallic contact at the source and drain, which can lead to different pinnings of the Fermi level and, consequently, to the formation of ohmic or Schottky contacts [6], [7]. The presence of Schottky-barrier (SB) contacts can have dramatic effects on device performance, because charge injection is subordinated to a tunneling process. However, in nanodevices with reduced oxide thickness, tunneling phenomena at the source and drain are favored, and while they often limit performance in conventional transistors, their exploitation is at the core of the concept of tunneling field-effect transistors (FETs) [8]. Indeed, theoretical investigations show that carbon-based tunneling FETs, such as the ones based on bilayer graphene [9] or epitaxial graphene on SiC substrates [10], can offer a potential route for low-power electronics beyond CMOS.

Transport in nanotransistors is certainly far from equilibrium but is still not fully ballistic, and currents are much lower than those predicted by ballistic models [11]. While it is perfectly clear that inelastic scattering may arise from the interaction of carriers with phonons and impurities, it is rather complex to take into account microscopically its effect on transport. A powerful phenomenological attempt to deal with carrier relaxation and decoherence was based on the Büttiker virtual probe approach [12], [13], in which inelastic scattering is thought as localized in special points, spaced by a length defined as "mean free path." The Büttiker approach was also introduced in microscopical models based on tight-binding Hamiltonians [14], and recently extended to deal, via a quantum Langevin approach, with 1-D conductors [15]. In [16], the Büttiker probe approach to inelastic scattering was employed in a simulation, based on the nonequilibrium Green's function formalism, of a nonballistic silicon nanowire transistor.

A fully microscopical analysis of inelastic scattering due to specific mechanisms such as phonon scattering, with the nonequilibrium Green's functions approach, has also been addressed by adding a proper self energy correction on a site-representation propagating Hamiltonian by Jin *et al.* [17] and Gilbert *et al.* [18], [19].

As far as analytical models are concerned, transport in quasi-1-D FETs is generally treated as purely ballistic or with a drift-diffusion assumption as in [20]–[22]. A largely invoked approach to treat partially ballistic transport, including the effects of backscattering, was proposed by Lundstrom [23]. This approach, which is easily included as a correction to ballistic models, has the merit of offering a very simple and synthetic picture but does not allow a full description of the seamless transition from ballistic to quasi-equilibrium drift-diffusion transport. Recently, a rigorous semianalytical model based on the Büttiker virtual probe approach [12], [13] has been conceived, in which a nonballistic transistor is seen as a suitable chain of N ballistic channels, where N is the ratio of the channel length to the mean free path, or, equivalently, as a series of a drift-diffusion FET and a ballistic FET [24]–[26].

In this paper, we propose a semianalytical model based on the virtual probe approach, which describes 1-D FETs, treating on equal footing SB contacts and far-from-equilibrium (FFE) transport conditions. In Section II, we summarize the general analytical description of GNR subbands, density of states,

Manuscript received August 24, 2009; revised March 18, 2010; accepted March 22, 2010. Date of publication May 24, 2010; date of current version June 23, 2010. This work was supported in part by the EC Seventh Framework Program through Project GRAND under Contract 215752, by the Network of Excellence Nanosil under Contract 216171, and by the European Science Foundation EUROCORES Program "Fundamentals of Nanoelectronics," funded by CNR and the EC Sixth Framework Program through Project Dewint under Contract ERAS-CT-2003-980409. The review of this paper was arranged by Editor M. J. Deen.

P. Michetti is with the Dipartimento di Ingegneria dell'Informazione, Universitá di Pisa, 56122 Pisa, Italy, and also with the Institute for Theoretical Physics and Astrophysics, University of Würzburg, 97070 Würzburg, Germany (e-mail: michetti@phisik.uni-wuerzburg.de).

G. Iannaccone is with the Dipartimento di Ingegneria dell'Informazione, Universitá di Pisa, 56122 Pisa, Italy (e-mail: g.inannaccone@iet.unipi.it).

Color versions of one or more of the figures in this paper are available online at http://ieeexplore.ieee.org.

Digital Object Identifier 10.1109/TED.2010.2049219

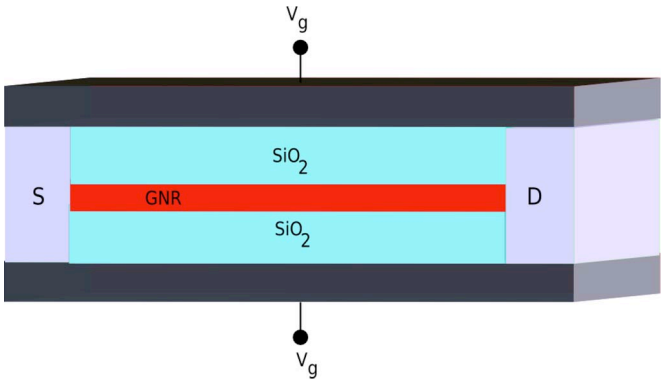

Fig. 1. Sketch of a DG-GNR FET, considered as an example for the application of our model.

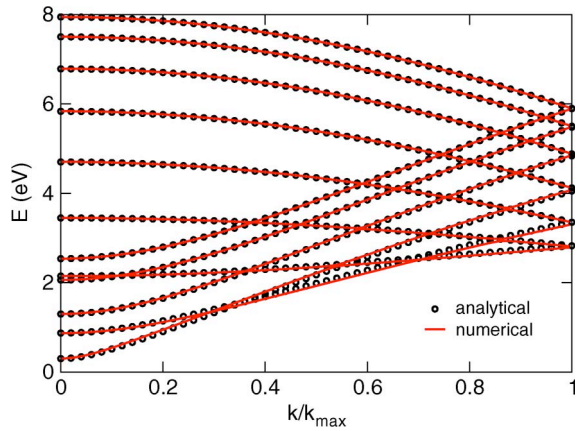

Fig. 2. Comparison of the subbands of an A-GNR with 12 dimer lines between a numerical tight-binding calculation and our analytical result with edge corrections. Valence bands are symmetrical.

and equilibrium charge density, extensible also to the CNT case. In Section III, we present a WKB approximation of the tunneling probability through SB contacts, yielding analytical expressions for the transmission based on two different levels of approximation for the energy dispersion curves of GNRs (or CNTs). In Section IV, a model for a single ballistic transistor with SB contacts is presented, compared with the data from numerical simulations. In Section V, we propose a compact model, based on the Büttiker virtual probe approach that is able to deal with both intermediate (I) transport and SB contacts, and use it to study the interplay of SB and dissipative transport.

II. Dispersion Relation and Density of States

The dispersion curve of an armchair GNR (A-GNR) with N dimer lines can be obtained analytically by cutting techniques, analogous to that used for CNTs in [27], from the 2-D graphene tight-binding dispersion. The subband dispersion curves correspond to 1-D segments of the graphene Brillouin zone with the confined wavevector quantized as $k_\alpha = \pi\alpha/(N+1)$, with $\alpha = 1, 2, \ldots, N$. The dispersion curve of the subband α, referred to as midgap, is

$$E_\alpha(k) = \pm V \left\{ 1 + 4\cos\frac{\sqrt{3}ak}{2} A_\alpha + 4A_\alpha^2 \right\}^{1/2} \tag{1}$$

with $A_\alpha = \cos(\pi\alpha/(N+1))$, and $V = 2.7$ eV is the tight-binding hopping parameter. We note here that a dispersion relation that is totally analogous to (1) applies to zigzag $(N, 0)$ CNT, with the only difference that, in the place of A_α, we have to use $A_\alpha^{\mathrm{CNT}} = \cos(\pi\alpha/N)$, where α is the subband index of CNTs [28]. Therefore, much of the results for GNRs obtained here and in the succeeding sections of this paper, with the exclusion of the edge corrections, can be directly generalized to the zigzag CNT case by properly modifying the values of parameters accounting for the screening and geometrical properties (Fig. 1).

The edge of the αth subband $E_\alpha(0)$ is expressed as

$$E_\alpha(0) = \pm V(1 + 2A_\alpha). \tag{2}$$

Let us note that the lowest lying subband is given by the value of α for which $A_\alpha + (1/2)$ is minimum. The edges of the nanoribbon are laterally exposed to vacuum and experience a different chemical environment; therefore, the hopping parameter between carbon atoms at the edges tends to be slightly different. We can, at least partially, account for the presence of edges via a perturbative approach to the first order [29]. The perturbation theory to the first order leads to the following eigenenergy corrections:

$$\begin{aligned}\delta E_\alpha(k) &= (\pm)_\alpha H^{\mathrm{ed}}_{\alpha,\alpha} \\ &= (\pm)_\alpha \frac{4\nu}{N+1} \sin^2\left(\frac{\alpha\pi}{N+1}\right) \cos(k a_{c-c})\end{aligned} \tag{3}$$

with $\nu = 0.12$ eV as the energy correction of the hopping parameter at the edges in the tight-binding Hamiltonian. The correction has a positive or negative contribution, depending on the wavefunction parity with respect to the two asymmetric carbon atoms, which are connected by the edges. Therefore, if $A_\alpha \geq -(1/2)$, we have a positive contribution $(\pm)_\alpha = 1$, otherwise a negative one $(\pm)_\alpha = -1$. The edge-corrected energy dispersion relation, which we will refer to as the full-band (FB) approximation when applied to FET modeling, is therefore

$$E^c_\alpha(k) = E_\alpha(k) + \delta E_\alpha(k). \tag{4}$$

The comparison between numerical tight-binding calculations, with edge effects taken into account, and the analytical result with perturbative corrections, for an A-GNR of 12 dimer lines, is shown in Fig. 2. The agreement is very good, particularly at $k = 0$, where (4) reproduces the results of [29]. For simplicity, we define here the band edges as $\varepsilon_\alpha = E^c_\alpha(0)$.

A. Approximated Expressions

In modeling nanotransistors, only the lowest laying subbands matter, in which the relevant transport phenomena take place. For these lowest lying subbands, often an effective-mass (EM) approximation is invoked

$$E^{\mathrm{EM}}_\alpha(k) = \varepsilon_\alpha + \frac{\hbar^2 k^2}{2M_\alpha} \tag{5}$$

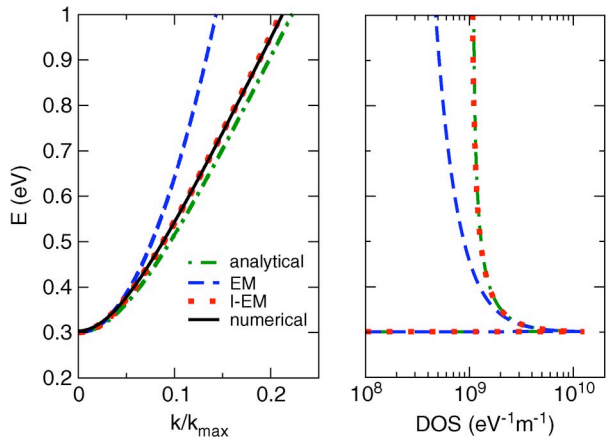

Fig. 3. Energy dispersion curve, and the corresponding density of states, of the lowest conduction subband of an A-GNR with 12 dimer lines. A numerical tight-binding result is compared with our FB analytical result and with EM and I approximate dispersions. In the energy range considered here, the agreement between numerical, FB, and I approximations is excellent.

in this case, the following EM for the αth mode can be employed

$$M_\alpha = -\frac{2}{3}\frac{\hbar^2\varepsilon_\alpha}{a^2V^2A_\alpha}. \tag{6}$$

The DOS in EM approximation is given by

$$D_\alpha^{\mathrm{EM}}(E) = \frac{2}{\pi\hbar}\sqrt{\frac{M_\alpha}{2E}} \tag{7}$$

with E expressing the "kinetic energy," i.e., the energy calculated with respect to the band edge ε_α.

The EM approximation is rather crude, and the following I approximation, between the FB and the EM, can be derived by expanding to the second order in k the energy squared of (4)

$$E_\alpha^I(k) = \pm\sqrt{\varepsilon_\alpha^2 + \frac{\varepsilon_\alpha\hbar^2k^2}{M_\alpha}} \tag{8}$$

for which the DOS is

$$D_\alpha^I(E) = \frac{2(\varepsilon_\alpha+E)}{\pi\hbar}\sqrt{\frac{M_\alpha}{\varepsilon_\alpha E\,(E+2\varepsilon_\alpha)}}. \tag{9}$$

In Fig. 3, we compare the lowest band dispersion curve and the corresponding DOS for a GNR with 12 dimer lines. Both the FB and I approximations reproduce numerical tight-binding calculations quite well and give similar DOS; of course, the I dispersion is only accurate for energies $E \ll V$. The EM approximation instead remains quite accurate only for about $E < 0.1$ eV.

B. Carrier Density

Carrier density affects both electrostatics and transport properties. Here, we develop a similar analysis to what was done in [28] for CNTs. The electron carrier density per subband can be expressed as

$$n_\alpha = \int_0^{\varepsilon_\alpha^{\mathrm{top}}-\varepsilon_\alpha} f\left(\frac{E+\varepsilon_\alpha-q\phi_c-\mu}{kT}\right)D_\alpha(E)\,dE \tag{10}$$

where μ is the Fermi level, $f(x) = (1+\exp x)^{-1}$ is the Fermi–Dirac distribution, and $\varepsilon_\alpha^{\mathrm{top}}$ is the top edge of the αth subband, which, for most purposes, can be taken as ∞ due to the finite extension of $f(E)$. ϕ_c is the electrostatic potential in the device, which rigidly shifts the levels. Because the nonnegligible contribution to (10) comes from states near ε_α, we can use the I expression for the DOS $D_\alpha^I(E)$. If we consider a nondegenerate situation ($\varepsilon_\alpha - 3kT > \mu$), typical of subthreshold regimes in FETs, we obtain

$$n_\alpha = \frac{2\sqrt{M_\alpha(\varepsilon_\alpha-q\phi_c)}}{\pi\hbar}\,e^{\beta(q\phi_c+\mu)}\int_1^\infty e^{-\beta(\varepsilon_\alpha-q\phi_c)z}\frac{z}{\sqrt{z^2-1}}\,dz \tag{11}$$

with $z = E/\varepsilon_\alpha$ and $\beta = (kT)^{-1}$. With a partial integration and recognizing the modified Bessel function of the second kind K_1, the charge density can be expressed as

$$n_\alpha = \frac{2}{\pi\hbar}\sqrt{M_\alpha\varepsilon_\alpha}e^{\beta(q\phi_c+\mu)}K_1(\beta\varepsilon_\alpha). \tag{12}$$

In order to give an estimation of the Bessel function K_1 which has no closed form, we can adopt the approximation [28]

$$K_1(x) \approx \frac{K_{1/2}(x)+K_{3/2}(x)}{2} = \sqrt{\frac{\pi}{2x^3}}\frac{1+2x}{2}e^{-x} \tag{13}$$

arriving in the end to express the charge density as

$$n = N_c e^{-\beta(\varepsilon_\alpha-q\phi_c-E_F)} \tag{14}$$

$$N_c = \sqrt{\frac{M_\alpha}{2\pi\beta^3}}\frac{1+2\beta\varepsilon_\alpha}{\hbar\varepsilon_\alpha} \tag{15}$$

with essentially the same form of 3-D bulk semiconductors.

III. Tunneling of SBs

Our aim is to provide an analytical description of the tunneling through SB contacts. The first step is to model in the simplest way the potential decay occurring near the source and drain contacts. The potential inside a transistor channel is described by the a 3-D Poisson equation

$$\nabla^2\phi(\vec{r}) = -\frac{\rho(\vec{r})}{\epsilon} \tag{16}$$

together with the boundary conditions enforced by voltages V_s, V_d, and V_g at the source, drain, and gate leads, respectively. In the evanescent mode analysis approach, the electrostatic potential inside a nanotransistor $\phi(\vec{r})$ is thought as the sum of a long-channel solution $\phi_L(\vec{r})$, which satisfies the vertical electrostatics, plus a short-channel solution $\phi^*(\vec{r})$, called evanescent mode, responsible of the potential variation along the channel [30]. The short-channel solution is obtained, solving the

Laplace equation for the device with an adequate expansion in harmonic functions. As a matter of fact, the short-channel solution near the source contact results in an exponential profile

$$\phi^*(\vec{r}) \propto R(\vec{r}_\parallel)e^{-z/\lambda} \tag{17}$$

where $R(\vec{r}_\parallel)$ describes the solution in the channel cross section and λ comes to be a natural scale length for the potential variation in the device. The actual value of λ depends on the details of the device geometry; however, in a double-gate (DG) configuration, and considering that, in general, in carbon-based FET, the oxide thickness is significantly larger than the channel thickness, the asymptotic value $\lambda = (2t_{\rm ox} + t_{\rm ch})/\pi$ can be assumed. In the case of a cylindrical GAA-CNT FET, an explicit calculation of λ via evanescent mode analysis has been performed in [31].

We follow this line and assume that the channel potential rigidly shifts the confinement eigenvalues ε_α, where α runs on the different subbands. Now, we are interested only in the potential inside the restricted zone of the graphene channel $\phi_c(z)$, in which it can be assumed as a constant (which is strictly true in subthreshold regimes), and we consider its variation only along the channel direction. The long-channel solution inside the channel is reduced to $\phi_L(\vec{r}) \approx \phi_c$, where ϕ_c is solely imposed by the vertical electrostatics, while the short-channel solution has the form (17). Therefore, the potential in the channel $\phi_c(z)$ can be expressed as

$$\phi_c(z) = \phi_c + \frac{A_s}{q}\, e^{-z/\lambda} \tag{18}$$

with $\phi_c = \phi(\infty)$ fixed by the vertical electrostatics and A_s imposed by the boundary condition at the SB contact $A_s = E_{\rm SB}^{(s)} - \varepsilon_L + q\phi_c$, where L refers to the lowest lying subband, due to the Fermi level pinning at the metal/semiconductor interface. $E_{\rm SB}^{(s)}$ is the SB height on the first conduction subband with respect to the source Fermi level. The charge injected from the source with energy lower than the barrier has to tunnel in order to reach the channel. We need to calculate the transmission through an exponential decaying barrier of the kind

$$E_{\rm SB}(z) = A_s\, e^{-z/\lambda} \tag{19}$$

with the height A_s dependent on the electrostatic potential ϕ_c. We note however that if the band bending exceeds the energy gap $2\varepsilon_\alpha$, a carrier with energy $0 < E < A_s - 2\varepsilon_\alpha$ will experience an SB of a height $A_s = E + 2\varepsilon_\alpha$.

In order to estimate the behavior of a nanotransistor, it is essential to accurately describe the tunneling phenomena, both in traditional FETs and in TFETs. In this section, we compare the tunneling calculated with WKB approximation in an FB approach (FB-WKB), within the EM approach (EM-WKB), and I approximation (I-WKB). FB-WKB is more complex to implement and requires a numerical solution of the integral

$$\ln\left(T(E)\right) = -2\int_{z_1}^{z_2} \mathcal{I}\left[k_z(zE)\right] dz. \tag{20}$$

While for the other two, an analytical expression for the tunneling $T(E)$ can be obtained.

A. EM-WKB Approximation

The transmission coefficient obtained via the WKB approximation is given as

$$T(E) = \begin{matrix} e^{-2\int_{z_1}^{z_2}\sqrt{2m_\alpha/\hbar^2(E_{\rm SB}(z)-E)}\,dz}, & E < A_s \\ 1, & E \geq A_s \end{matrix} \tag{21}$$

where z_1 and z_2 are the classical turning points

$$z_1 = 0 \qquad z_2 = -\lambda \ln\left[\frac{E}{A_s}\right]. \tag{22}$$

The transmission coefficient can be analytically calculated in

$$\ln T(E) = -4\lambda\sqrt{\frac{m_\alpha(A_s - E)}{\hbar^2}} \times \left[1 - \sqrt{\frac{E}{A_s - E}}\tan^{-1}\left(\sqrt{\frac{A_s - E}{E}}\right)\right]. \tag{23}$$

B. I-WKB Approximation

Let us consider a dispersion curve of the kind (8). The turning points with a barrier like (19) are the same as (22), but now, under the barrier, the imaginary part of the wave vector as a function of energy is given by

$$\mathcal{I}[k_z, E] = \sqrt{\frac{M_\alpha}{\hbar^2\varepsilon_\alpha}}\sqrt{a^2 - \left(b - e^{-\frac{z}{\lambda}}\right)^2} \tag{24}$$

with

$$a = \frac{\varepsilon_\alpha}{A_s} \qquad b = a + \frac{E}{A_s}.$$

The integration (20), for $E < A_s$, leads to the WKB tunneling probability

$$\ln T(E) = \frac{2A_s\lambda\sqrt{M_\alpha}}{\sqrt{\hbar^2\varepsilon_\alpha}}\left[-b\left(\frac{\pi}{2} - \arctan\frac{b-1}{R_1}\right) - R_1 + R_2\left(\pi - \arctan\frac{R_1R_2}{a^2 - b^2 + b}\right)\right] \tag{25}$$

where we introduced the abbreviations

$$R_1 = \sqrt{a^2 - (b-1)^2} \qquad R_2 = \sqrt{b^2 - a^2}.$$

C. FB-WKB Approximation

For an A-GNR, subband dispersion curves are in the form (1), from which we can express the wave vector as a function of energy as

$$k = \frac{2}{a\sqrt{3}}\arccos x \tag{26}$$

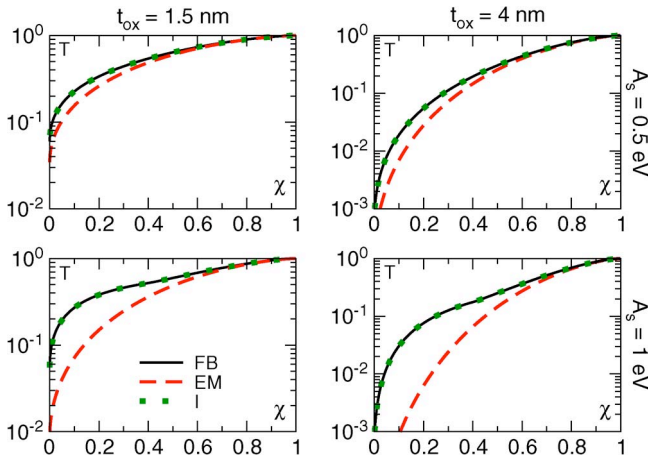

Fig. 4. Transmission probability for an electron in the lowest laying subbands of an A-GNR with 12 dimer lines as a function of its relative energy χ with respect to the barrier height. The FB result comes from the numerical integration of (29), while we have analytical transmission probability in I (25) and EM (23) approximations.

with the substitution $u = -z/\lambda$ and normalizing all quantities to A, x given by

$$x = \frac{\left(\frac{E}{A_s} + \delta - e^u\right)^2 - \alpha^2}{\nu}$$

where we introduced

$$\delta = \frac{\varepsilon_\alpha}{A_s} \qquad \alpha = \frac{\left(1 + 4A_\alpha^2\right) V^2}{A_s^2} \qquad \nu = \frac{4A_\alpha V^2}{A_s^2}. \tag{27}$$

In the integration domain of (20), the argument x of the inverse cosine function has a module larger than one, and therefore

$$\mathcal{I}(k) = -\frac{2}{a\sqrt{3}} \ln\left|z + \sqrt{z^2+1}\right| \tag{28}$$

leading to the WKB tunneling probability

$$\ln T(E) = -\frac{4\lambda}{a\sqrt{3}} \int_0^{\ln E/A_s} \ln\left|x + \sqrt{x^2+1}\right| du. \tag{29}$$

In Fig. 4, we compare the tunneling coefficients, calculated with the EM-, I-, and FB-WKB approaches, for SBs of height 0.5 and 1 eV, and for a λ typical of DG A-GNR with $t_{\rm ox} =$ 1.5 and 4 nm. Essentially, the I approximation completely reproduces the FB tunneling probability, while a significant deviation is observed with the EM-WKB approximation for $E < 0.5A_s$. Therefore, the I approximation seems an optimal approximation for compact models in order to reduce the computational times, retaining high accuracy.

IV. SB Ballistic FET

We consider here a ballistic transistor with SB contacts at the source and drain, as shown in Fig. 5. As usual in compact models, we assume a complete phase randomization along the channel, neglecting phase resonances in the transmission probability of the two tunneling barriers, while multiple reflection

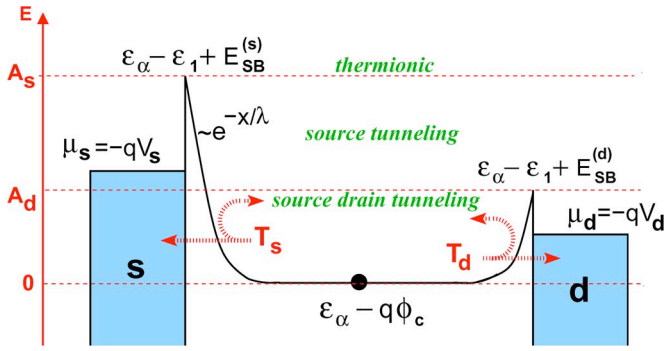

Fig. 5. Conduction band edge profile of an SB nanoscale FET. The thermionic and tunneling energy ranges are shown.

events are taken into account. Between two tunneling barriers, the forward and backward distribution functions are modified by the multiple elastic scattering [31], [32]. The overall mobile charge, given by the sum of forward- and backward-going charge carriers in the channel, can be expressed as

$$\frac{Q_i}{q} = \sum_\alpha \int_0^{\varepsilon_\alpha^{\rm top} - \varepsilon_\alpha} dE D_\alpha(E) \left\{ \frac{T_s(2 - T_d)}{T^*} f\left(\eta_{\alpha,s}^i\right) + \frac{T_d(2 - T_s)}{T^*} f\left(\eta_{\alpha,d}^i\right) \right\} \tag{30}$$

with $i = e, h$ for the electron and hole charge, where

$$\eta_{\alpha,s(d)}^e = \frac{E - q\phi_c + \varepsilon_\alpha - \mu_{s(d)}}{k_b T} \tag{31}$$

$$\eta_{\alpha,s(d)}^h = \mu_{s(d)} - E + q\phi_c - \varepsilon_\alpha k_b T \tag{32}$$

$$T^* = T_s + T_d - T_s T_d \tag{33}$$

where T_s and T_d are the tunneling coefficients at the source and drain, respectively, depending on both energy and channel potential. In order to compute the channel potential ϕ_c, and, through it, the subband energies, the total mobile charge $Q = Q_h - Q_e$ must be equal to the charge induced by the electrostatic coupling of channel with gate, source, and drain through capacitances C_g, C_s, and C_d, respectively

$$Q(\phi_c) = -\sum_{i=g,s,d} C_i(V_i - V_{{\rm FB},i} - \phi_c) \tag{34}$$

where $V_{{\rm FB},i} = \phi_i - \chi_g$ is the flatband voltage, given by the difference between the contact workfunction and the graphene electron affinity.

The current is obtained with the Landauer–Büttiker formalism, which, accounting for the tunneling, takes the following form:

$$I_i(\phi_c) = \frac{q}{\pi\hbar} \sum_\alpha \int_0^{E_\alpha^{\rm top} - \varepsilon_\alpha} \frac{T_s T_d}{T^*} \left[f\left(\eta_{\alpha,s}^i\right) - f\left(\eta_{\alpha,d}^i\right) \right] dE \tag{35}$$

with $i = e, h$ accounting for the current of electrons and holes, and the total current given by $I = I_e - I_h$. We note that (30) and (35) include both tunneling and thermionic contributions.

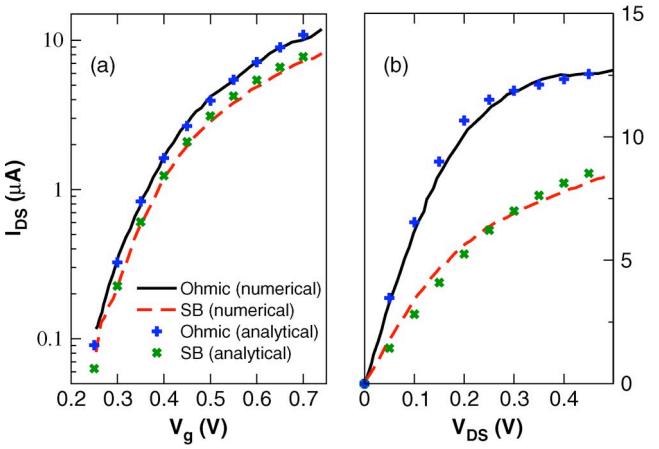

Fig. 6. Comparison between our model and numerical simulations from [33]. The (a) transfer characteristics at $V_{\rm ds} = 0.5$ V and (b) output characteristics at $V_g = 0.75$ V of a ballistic DG A-GNR FET, with ohmic and SB contacts of height $E_g/2 \approx 0.3$ eV, are shown. Assuming a GNR thickness of about 1 nm, we obtain $\lambda \approx 1.3$ nm.

We apply our model to the case of a DG A-GNR transistor (DG A-GNR FET) with both ohmic and SB contacts. In Fig. 6, we compare the (a) transfer and (b) output characteristics of a ballistic A-GNR FET, obtained with our model and with numerical simulations based on the nonequilibrium Green's function formalism in [33]. The SiO_2 gate oxide thickness is 1.5 nm, and the A-GNR lattice is characterized by 12 dimer lines, which correspond to a width of 1.35 nm and a bandgap of 0.6 eV. We employed here the I analytical description of the GNR subbands and density of states (9). The source and drain capacitances C_s and C_d are introduced because of the short-channel nature of the GNR simulated in [33] and are fixed, with respect to the gate capacitance $C_g = 1.1 \times 10^{-10}$ F/m, to $C_s = C_d = 0.1C_g$. The agreement between the numerical simulations and our compact model, for both curves (Fig. 6) with ohmic and SB contacts, is very good, demonstrating that the effects of SBs are well accounted for.

V. SB Transistors in I Transport Regime

To describe dissipative transport, we follow the approach developed in [24] and [25] for a 2-D MOSFET for the nondegenerate and degenerate cases, and in [26] for quasi-1-D FETs. Such treatment is here expanded to include ambipolar devices. We recall that, within the Büttiker probe approach, inelastic scattering is thought as localized in special points, spaced by a length defined as "mean free path" ℓ. The virtual probes act as localized reservoirs along the channel, in which carriers are fully thermalized in equilibrium with the probe quasi-Fermi energy μ_n. The transport from one virtual probe to the next is considered purely ballistic. We have a drift-diffusion transistor when the channel length is much longer than the mean free path, which, from our point of view, is equivalent to having a long enough chain of ballistic transistors, as rigorously shown in [24]. On the contrary, when the number of internal contacts is small, the transport is FFE and is fully ballistic in the limit $N = 1$.

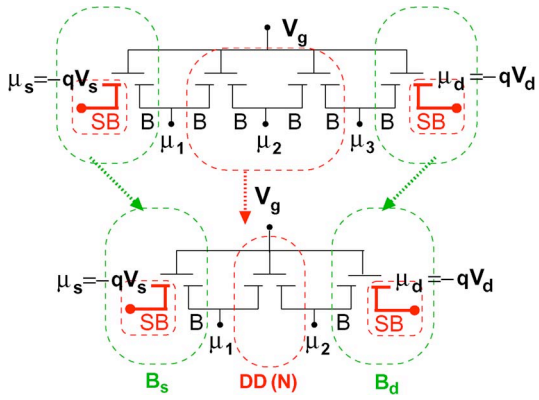

Fig. 7. Chain of N ballistic transistors with SB contacts at the source and drain (first and last contacts). As explained in the text, the chain of ballistic transistors can be described as the series made by a central DD section accounting for dissipative transport in the $N-2$ internal nodes and by head and tail ballistic transistors accounting for the SB contacts with source and drain.

A transistor with SB contacts in the FFE transport regime is therefore modeled as a series of individually ballistic channels, connected by fully thermalizing virtual probes placed at $x_n = n\ell$ with $n = 1, \ldots, N-1$, with electrochemical potential μ_n. The head and tail of the series are connected to the source and drain through SB contacts, as shown in Fig. 7, and boundaries are fixed as $\mu_0 = \mu_s$ and $\mu_N = \mu_d$. In the nth ballistic channel, μ_{n-1} and μ_n act as source and drain, and by simultaneously solving (30) and (34), we can fix the channel potential $\phi_c^{(n)}$. In the same manner, the current in the nth channel is obtained with (35), imposing μ_{n-1} and μ_n as source and drain Fermi levels. Since the current I_n in any $n = 1, \ldots, N$ FET must be equal to $I_{\rm ds}$, we have N equations determining the local Fermi energies μ_n. We note that a distinction between ballistic internal channels (B) and boundary channels with source (B_s) and drain (B_d) can be made. In fact, the first and the last ballistic channels are characterized by SB contacts with metallic source and drain, while internal channels, in the region between the fictitious virtual probes, can be treated as ohmic transistors. The numerical solution of the complete chain of N elements (2 for the boundary kind and $N-2$ for the internal kind) will be addressed as the $B(N)$ model.

Now, we note that, for the internal part of the chain, the analysis developed in [26] applies. In particular, it has been shown that the current in an ohmic-contact ballistic chain of N elements, after a linearization procedure, can be arranged into a drift-diffusion-like form (which we refer to as the $DD(N)$ model) in which the current is calculated through the following formula:

$$I_{\rm ds} = \frac{q^2\Gamma(1)\ell}{\pi\hbar L}\sum_{\alpha}\int_{V_s}^{V_d}\left\{F_{-1}\left(\eta_\alpha^e[V]\right) - F_{-1}\left(\eta_\alpha^h[V]\right)\right\}dV \quad (36)$$

where $F_{-1}(x)$ is the Fermi–Dirac integral of order -1, Γ is the gamma function, and

$$\eta_\alpha^e = (q\phi_c - qV - \varepsilon_\alpha)/kT \quad (37)$$

$$\eta_\alpha^h = (-q\phi_c + qV + \varepsilon_\alpha)/kT. \quad (38)$$

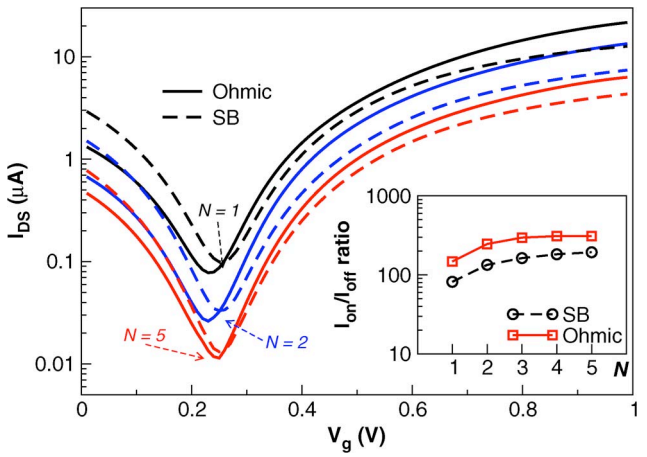

Fig. 8. Transfer characteristics of a ballistic chain made of a series of N DG GNR FETs, with $N = 1, 2, 5$ and $V_{\rm ds} = 0.5$ V, calculated with our model. In the inset, the $I_{\rm on}/I_{\rm off}$ ratio for $V_g^{(\rm off)} = 0.25$ V and $V_g^{(\rm on)} = 0.75$ V as a function of N.

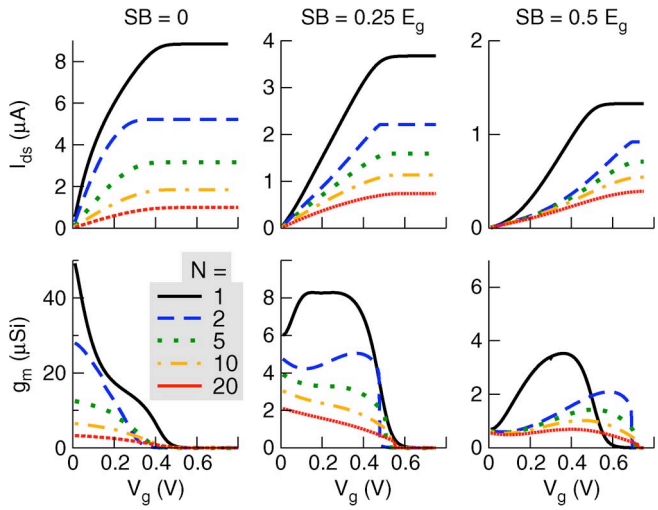

Fig. 9. Output characteristics and differential conductance of a GNR ballistic chain made of N DG GNR FETs, with $N = 1, 2, 5, 10, 20$. Three different pinnings of the SB with respect to the conduction band are considered: Without SB ($SB = 0$) and with SBs of $E_g/4$ and $E_g/2$. The details of the device are the same as those in Fig. 6, except for $t_{\rm ox} = 5$ nm, for which all the features due to the SB are enhanced due to the thicker barrier.

We note that η not only directly depends on V but also indirectly through ϕ_c, which is self-consistently imposed by the linearized vertical electrostatics

$$Q_m = C_g\,(V_g - V_{\rm FB} - \phi_c[V])$$

$$Q_m = -\frac{q\Gamma(1/2)}{\pi}\sum_\alpha \sqrt{\frac{2k_bTm_\alpha}{\hbar^2}}\left\{F_{1/2}(\eta_\alpha^e[V]) - F_{1/2}\left(\eta_\alpha^h[V]\right)\right\}.$$

The linearized DD model (36) has also the advantage of dealing with noninteger $N = L/\ell$ and is therefore more flexible than the ballistic chain itself. As noted in [26], (36) can be rearranged in a local form, analogous to a DD equation $I_\alpha = \mu_\alpha Q_\alpha (dV/dx)$, where the degenerate mobility (we consider now a monopolar regime) is given by

$$\mu_\alpha^e = \frac{q\nu_\alpha \ell}{2kT}\frac{F_{-1}\left[\eta_\alpha^e\right]}{F_{-1/2}\left[\eta_\alpha^e\right]} \tag{39}$$

with $\nu_\alpha = \sqrt{2kT/\pi m_\alpha}$ as the mean carrier velocity. This expression gives us a link between $N = L/\ell$ and the mobility.

We can now model an SB transistor in I transport regime as a series of $B_s - DD(N) - B_s$ segments, with two nodes between the boundary channels and the internal segment, characterized by electrochemical potentials that can be fixed by exploiting the current continuity in the device. We will refer to this macromodel as the $BDDB(N)$ model. This compact model permits one to analyze both the presence of SB contacts and FFE transport condition, while keeping low the computational burden, particularly with respect to numerical simulations including dissipation.

We now analyze the effects of inelastic scattering on the performance of a DG A-GNR FET. In nonballistic transport (increasing N), the transfer characteristics (Fig. 8) vertically shift, in a semilog plot, as expected, due to mobility reduction. It is interesting to note that the effect is more marked in the subthreshold region and, consequently, an increase of the $I_{\rm on}/I_{\rm off}$ ratio as a function of N is observed, as shown in the inset. In ballistic models with positive $V_{\rm ds}$, in the subthreshold regime, tunneling from the drain leads to hole accumulation under the channel, which increases the quantum capacitance and reduces the control over channel. Subsequently, a larger subthreshold swing and a lower $I_{\rm on}/I_{\rm off}$ are obtained.

An accurate analysis of the SB effects on the output characteristics can be performed by calculating the differential conductance $g = \partial I_{\rm ds}/\partial V_{\rm ds}$. In Fig. 9, we compare the output characteristics and the differential conductance for a device with $t_{\rm ox} = 5$ nm with an SB height $SB = 0, 0.25, 0.5\ E_g$. Note that the presence of SB contacts is more relevant in transistors with a looser vertical confinement, where the tunneling barriers are thicker. We observe that, in samples with $SB = 0$ eV, the output characteristics concavity is always negative, and the differential conductance is monotonously decreasing with $V_{\rm ds}$. If the SB height is finite, the differential conductance acquires a nonmonotonous behavior, which well describes the "S-shaped" concavity change of the characteristics curves before reaching saturation, particularly evident in thicker SB devices. It is interesting to note that, apart from a reduction of the maximum saturation current, larger ballistic chains (larger N), in which higher inelastic scattering is active, lead to smoothening of the nonmonotonous dependence of g on $V_{\rm ds}$. With this fact, we can recognize a gradual transition between devices in which the characteristics are dominated by SB contacts and devices in which inelastic relaxation is predominant.

In electron–hole symmetrical materials as undoped GNRs or CNTs, the relative SB height with respect to the bandgap determines the position of the minimum of transfer characteristics, and it influences their shape and symmetry (see Fig. 10). An SB of height $E_g/2$ preserves the band-structure electron–hole symmetry and therefore results in transfer characteristics which span symmetrically from the current minimum OFF state (placed at $V_g = V_{\rm ds}/2$). Curves calculated with reduced SB height for electrons (for $E_g/4$ and 0) show a growing asymmetry, with weaker hole currents and larger electron

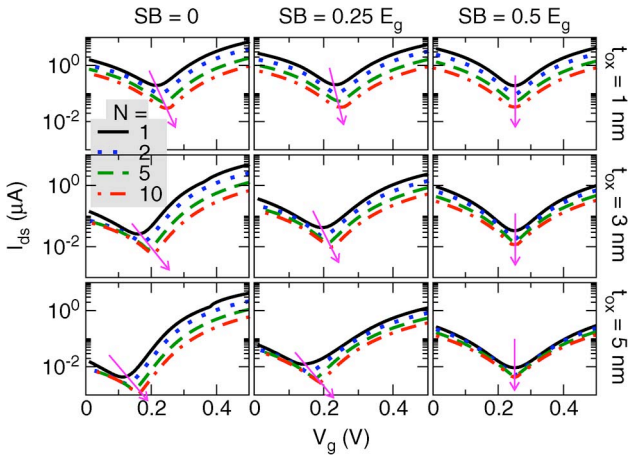

Fig. 10. Transfer characteristics of GNR devices increasing $t_{\rm ox} = 1, 3, 5$ nm, calculated for $V_{\rm ds} = 0.5$ V. Ballistic chains of $N = 1, 2, 5, 20$ are drawn; devices without SB ($SB = 0$) and with SBs of $E_g/4$ and $E_g/2$ are shown. Arrows indicating the shift of the transfer characteristics curves with N are also added as a guide for the eyes.

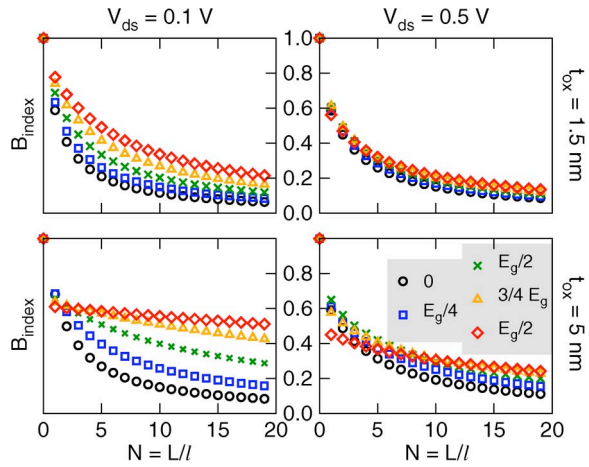

Fig. 11. Ballistic index of a ballistic chain of N elementary GNR FETs with SB is varied from 0 to $E_g/2$ as a function of N. The source–drain voltage is set to $V_{\rm ds} = 0.1$ and 0.5 V for $V_g = 0.75$ V.

currents, together with a shift of the transfer characteristic minimum to lower values of V_g. This phenomenon is prominent in thicker SB devices, such as the $t_{\rm ox} = 5$ nm FET, but well observable also in a $t_{\rm ox} = 1$ nm device. The increase of the lateral confinement leads in fact to an almost linear increase of the SB thickness, and therefore, all tunneling processes become harder. As expected, if we increase the dissipative phenomena (increasing N), a reduction of the current is observed. More interestingly, while the $SB = E_g/2$ curves vertically shift, as pointed out with the arrows in Fig. 10, while the shift of the other curves is diagonal; note, in fact, the horizontal shift of their minima with N. Moreover, by increasing N, the minima seem to converge toward the value $V_g = V_{\rm ds}/2$, which is typical of a symmetrical ambipolar device. This is yet another signature of the growing importance of inelastic transport over the SB contacts. Therefore, for sufficiently well-confined FET, we can expect in quasi-ballistic GNT/CNT devices to clearly observe an SB behavior, which becomes more and more subtle in dissipative regimes. To quantify the relative importance of the SB in determining the symmetry of the transfer characteristics, we made the following physical estimation: $SB = 0.5E_g$ corresponds to the symmetrical case; therefore, if we impose a different SB, the change in the conductance will be exponential in the SB difference $\delta E_{\rm SB}$ as

$$\delta g_{\rm SB} \propto \exp\left\{-\frac{2t_{\rm ox}}{\pi\hbar}(2m\delta E_{\rm SB})^{1/2}\right\} \tag{40}$$

as can be obtained estimating the differential conductance of a device with an SB source contact at the source Fermi level. This quantity is, in fact, dominated by the tunneling coefficient (23). This difference in the conductance is relevant as long as it is greater than the conductance due to the DD(N) chain. We obtain

$$\gamma = \frac{\delta g_{\rm SB}}{g_N} \approx N \exp\left\{-t_{\rm ox} * \frac{2}{\pi\hbar}(2m\delta E_{\rm SB})^{1/2}\right\}. \tag{41}$$

Employing this formula, we can calculate the $N = N_s$ corresponding to $\gamma = 1$ for different SB values and oxide thicknesses, as shown in the following table:

N_s	$t_{\rm ox} = 1$	$t_{\rm ox} = 3$	$t_{\rm ox} = 5$ (nm)
$SB = 0$	4	70	10^3
$SB = 0.25E_g$	7	450	10^4

.

N_s gives a rough estimation to the number of nodes (i.e., L/ℓ ratio) needed to make the transfer characteristics symmetrical, in spite of the presence of an SB. As can be observed, comparing these values with the behavior of the curves in Fig. 10, the $t_{\rm ox} = 1$ nm curves with $SB = 5$ and 10, respectively, for $SB = 0.25E_g$ and 0 are quite symmetrical in accordance with $N_s = 4$ and $N_s = 7$ found by our calculation. The minimum of the curve $N = 10$ with $SB = 0.25E_g$ comes near the symmetrical values, but still misses it, being our estimation $N_s = 70$. Other curves are highly asymmetric, being $N \ll N_s$.

A typical parameter used to characterize the transport regime in quasi-ballistic devices is the ballisticity index $B_{\rm index} = I/I_1$, which is the ratio of the actual current to the current corresponding to an analogous device in a purely ballistic transport regime ($N = 1$). In Fig. 11, we analyze the role of the SB contacts in determining the ballisticity index as a function of N and, therefore, as a function of the degree of inelastic relaxation. In general, to lower SB heights corresponds to a faster variation of $B_{\rm index}$ with N, with a sudden drop of the ballisticity as a function of the number of nodes, after which a slower decrease is observed. SBs affect, in particular, the ballisticity index calculated for lower $V_{\rm ds}$, due to the concavity of the output characteristics, while larger source–drain voltages reduce the relative importance of SB with respect to inelastic mechanisms. Calculations with $t_{\rm ox} = 5$ nm reveal the increased importance of SB contacts and reflect the presence of the inflection in the output characteristics, with a concavity change before saturation. In particular, for higher value of the SB, we observe a slower dependence of the $B_{\rm index}$ on N, because the current is calculated in a bias point of the characteristic curve of strong "s" curvature. Physically, it means that the current

flowing in the device is mostly limited by the injection through the tunneling barriers.

VI. Conclusion

We have presented a semianalytical model dealing with ambipolar 1-D SB transistors in I transport regimes between fully ballistic and quasi-equilibrium, i.e., governed by the drift-diffusion model. We have introduced simplified, but accurate, descriptions of the SB profiles and of the electrostatics, and analytical approximations of the tunneling coefficients of the SBs. We have demonstrated that an SB transistor can be modeled as three transistors in series, with common gate voltage. The central one is a drift-diffusion transistor, with mobility dependent on the degree of degeneracy of the 1-D carrier gas. The other two transistors are ballistic FETs with an SB contact corresponding to the external actual contacts (source or drain). In the case of ballistic transport, our model allows us to reproduce the results of a 3-D numerical Poisson–Schroedinger simulator. In the case of very long channel, with respect to the mean free path, current is limited by the central drift-diffusion transistor. The model allows one very directly to investigate the transition from barrier- to channel-limited transport. Our semianalytical model represents an accurate and simple way to gain physical insights into the behavior of nanoscale transistors with SB contacts, including most the relevant physics at a very low computational cost. We also developed an open-version tool, which is available on the Nanohub site under the name *FFETtool* [34], solving the model discussed in this paper, restricted to the EM approximation.

References

[1] K. S. Novoselov, A. K. Geim, S. V. Morozov, D. Jiang, Y. Zhang, S. V. Dubonos, I. V. Grigorieva, and A. A. Firsov, "Electric field effect in atomically thin carbon films," *Science*, vol. 306, no. 5696, pp. 666–669, Oct. 2004.

[2] K. S. Novoselov, A. K. Geim, S. V. Morozov, D. Jiang, M. I. Katsnelson, I. V. Grigorieva, S. V. Dubonos, and A. A. Firsov, "Two-dimensional gas of massless Dirac fermions in graphene," *Nature*, vol. 438, no. 7065, pp. 197–200, Nov. 2005.

[3] A. K. Geim and K. S. Novoselov, "The rise of graphene," *Nature Mater.*, vol. 6, no. 3, pp. 183–191, Mar. 2007.

[4] A. Bachtold, P. Hadley, T. Nakanishi, and C. Dekker, "Logic circuits with carbon nanotube transistors," *Science*, vol. 294, no. 5545, pp. 1317–1320, Nov. 2001.

[5] X. Li, X. Wang, L. Zhang, S. Lee, and H. Dai, "Chemically derived, ultrasmooth graphene nanoribbon semiconductors," *Science*, vol. 319, no. 5867, pp. 1229–1232, Feb. 2008. 1150878.

[6] A. Javey, J. Guo, Q. Wang, M. Lundstrom, and H. Dai, "Ballistic carbon nanotube field-effect transistors," *Nature*, vol. 424, no. 6949, pp. 654–657, Aug. 2003.

[7] Z. Zhou, G. Eres, R. Jin, A. Subedi, D. Mandrus, and E. Kim, "The performance of *in situ* grown Schottky-barrier single wall carbon nanotube field-effect transistors," *Nanotechnology*, vol. 20, no. 8, p. 085709, Feb. 2009.

[8] J. Knoch and J. Appenzeller, "Tunneling phenomena in carbon nanotubes field-effect transistors," *Phys. Stat. Sol. (A)*, vol. 205, no. 4, pp. 679–694, Apr. 2008.

[9] G. Fiori and G. Iannaccone, "Ultralow-voltage bilayer graphene tunnel FET," *IEEE Electron Device Lett.*, vol. 30, no. 10, pp. 1096–1098, Oct. 2009.

[10] P. Michetti and G. Iannaccone, "Model of tunneling transistors based on graphene on SiC," *Appl. Phys. Lett.*, vol. 96, no. 13, p. 133 508, Mar. 2010.

[11] N. Singh, A. Agarwal, L. Bera, T. Liow, R. Yang, S. Rustagi, C. Tung, R. Kumar, G. Lo, N. Balasubramanian, and D. Kwong, "High-performance fully depleted silicon nanowire (diameter $\leq$ 5 nm) gate-all-around CMOS devices," *IEEE Electron Device Lett.*, vol. 27, no. 5, pp. 383–386, May 2006.

[12] M. Büttiker, "Small normal-metal loop coupled to an electron reservoir," *Phys. Rev. B, Condens. Matter*, vol. 32, no. 3, pp. 1846–1849, Aug. 1985.

[13] M. Büttiker, "Role of quantum coherence in series resistors," *Phys. Rev. B, Condens. Matter*, vol. 33, no. 5, pp. 3020–3026, Mar. 1986.

[14] J. L. D'Amato and H. M. Pastawski, "Conductance of a disordered linear chain including inelastic scattering events," *Phys. Rev. B, Condens. Matter*, vol. 41, no. 11, pp. 7411–7420, Apr. 1990.

[15] D. Roy and A. Dhar, "Electron transport in a one dimensional conductor with inelastic scattering by self-consistent reservoirs," *Phys. Rev. B, Condens. Matter*, vol. 75, no. 19, p. 195 110, May 2007.

[16] J. Wang, E. Polizzi, and M. Lundstrom, "A three-dimensional quantum simulation of silicon nanowire transistors with the effective-mass approximation," *J. Appl. Phys.*, vol. 96, no. 4, pp. 2192–2203, Aug. 2004.

[17] S. Jin, Y. Park, and H. S. Min, "A three-dimensional simulation of quantum transport in silicon nanowire transistor in presence of electron–phonon interactions," *J. Appl. Phys.*, vol. 99, no. 12, p. 123 719, Jun. 2006.

[18] M. Gilbert, R. Akis, and D. Ferry, "Phonon-assisted ballistic to diffusive crossover in silicon nanowire transistor," *J. Appl. Phys.*, vol. 98, no. 9, p. 094303, Nov. 2005.

[19] M. Gilbert and S. Banerjee, "Ballistic to diffusive crossover in III–IV nanowire transistors," *IEEE Trans. Electron Devices*, vol. 54, no. 4, pp. 645–653, Apr. 2007.

[20] D. Jiménez, J. Sáenz, B. Iniguez, J. Suné, L. Marsal, and J. Pallarés, "Unified compact model for the ballistic quantum wire and quantum well metal–oxide–semiconductor field-effect-transistor," *J. Appl. Phys.*, vol. 94, no. 2, pp. 1061–1068, Jul. 2003.

[21] D. Jiménez, B. Iniguez, J. Suné, L. Marsal, J. Pallarés, J. Roig, and D. Flores, "Continuous analytic I–V model for surrounding-gate MOSFETs," *IEEE Electron Device Lett.*, vol. 25, no. 8, pp. 571–573, Aug. 2004.

[22] B. Paul, R. Tu, S. Fujita, M. Okajima, T. Lee, and Y. Nishi, "An analytical compact circuit model for nanowire FET," *IEEE Trans. Electron Devices*, vol. 54, no. 7, pp. 1637–1644, Jul. 2007.

[23] M. Lundstrom, "Elementary scattering theory of the Si MOSFET," *IEEE Electron Device Lett.*, vol. 18, no. 7, pp. 361–363, Jul. 1997.

[24] G. Mugnaini and G. Iannaccone, "Physics-based compact models of nanoscale MOSFETs. Part I: Transition from drift-diffusion to ballistic transport," *IEEE Trans. Electron Devices*, vol. 52, no. 8, pp. 1795–1801, Aug. 2005.

[25] G. Mugnaini and G. Iannaccone, "Physics-based compact models of nanoscale MOSFETs. Part II: Effects of degeneracy on transport," *IEEE Trans. Electron Devices*, vol. 52, no. 8, pp. 1802–1806, Aug. 2005.

[26] P. Michetti, G. Mugnaini, and G. Iannaccone, "Analytical model of nanowire FETs in a partially ballistic or dissipative transport regime," *IEEE Trans. Electron Devices*, vol. 56, no. 7, pp. 1402–1410, Jul. 2009.

[27] J. W. Mintmire and C. T. White, "Universal density of states for carbon nanotubes," *Phys. Rev. Lett.*, vol. 81, no. 12, pp. 2506–2509, Sep. 1998.

[28] D. Akinwande, T. Nishi, and H.-S. Wong, "Analytical derivation of the density of states, effective mass, and carrier density for achiral carbon nanotubes," *IEEE Trans. Electron Devices*, vol. 55, no. 1, pp. 289–297, Jan. 2008.

[29] Y.-W. Son, M. Cohen, and S. Louie, "Energy gaps in graphene nanoribbons," *Phis. Rev. Lett.*, vol. 97, no. 21, p. 216 803, Nov. 2006.

[30] S.-H. Oh, D. Monroe, and J. Hergenrother, "Analytical description of short-channel effects in fully-depleted double-gate and cylindrical surrounding-gate MOSFETs," *IEEE Electron Device Lett.*, vol. 21, no. 9, pp. 445–447, Sep. 2000.

[31] A. Hazeghi, T. Krishnamohan, and H.-S. Wong, "Schottky-barrier carbon nanotube field-effect transistor modeling," *IEEE Trans. Electron Devices*, vol. 54, no. 3, pp. 439–445, Mar. 2007.

[32] M. Büttiker, "Coherent and sequential tunneling in series barriers," *IBM J. Res. Develop.*, vol. 32, no. 1, pp. 63–75, Jan. 1988.

[33] Y. Yoon, G. Fiori, S. Hong, G. Iannacone, and J. Guo, "Performance comparison of graphene nanoribbon FETs with Schottky contacts and doped reservoirs," *IEEE Trans. Electron Devices*, vol. 55, no. 9, pp. 2314–2323, Sep. 2008.

[34] P. Michetti and G. Iannaccone, Model for Far From Equilibrium Transport in CNT/GNR FETs, 2009. [Online]. Available: http://nanohub.org/resources/ffettool

Paolo Michetti received the M.S. degree in material science and the Ph.D. degree in physics from the Universitá di Pisa, Pisa, Italy, in 2004 and 2008, respectively. His Ph.D. was devoted to theoretical investigation of the optical properties of organic nanostructured materials, like J-aggregate microcavities in strong light-matter coupling regime, particularly focusing on the effects of disorder and the modeling of their photoexcitation dynamics.

Since 2008, he has been with the Dipartimento di Ingegneria dell'Informazione: Elettronica, Informatica, Telecomunicazioni, Universitá di Pisa, focusing on the modeling of nanoelectronic devices, based on nanowires, nanotubes, and graphene nanoribbons. He is also with the Institute for Theoretical Physics and Astrophysics, University of Würzburg, Würzburg, Germany.

Giuseppe Iannaccone (M'98–SM'10) received the M.S. and Ph.D. degrees in electrical engineering from the Universitá di Pisa, Pisa, Italy, in 1992 and 1996, respectively.

In 1996, he took a permanent position as a Researcher with the Italian National Research Council, and in the same year, he obtained a faculty position at the Electrical Engineering Department, Universitá di Pisa, as an Assistant Professor, where he has been an Associate Professor of electronics since January 2001. His interests include transport and noise in nanoelectronic and mesoscopic devices, development of device modeling and TCAD tools, and the design of extremely low-power circuits and systems for RFID and ambient intelligence scenarios. He has authored and coauthored more than 120 papers published in peer-reviewed journals and more than 80 papers in proceedings of international conferences.

Dr. Iannaccone has coordinated a few European and National Projects involving multiple partners and has acted as the Principal Investigator in several research projects funded by public agencies at the European and National levels and by private organizations. He is in the technical committee of few international conferences and serves as a Referee for the leading journals in the fields of condensed-matter physics, device electronics, and circuit design.